RSC Advances

PAPER

View Article Online
View Journal | View Issue

Cite this: *RSC Adv.*, 2024, **14**, 7430

Coordination-induced and tunable layered rare-earth hydroxide-complex intercalated nanohybrid phosphorescent photosensitizer and therapy†

Zhongli Zhao, *[ab] Hailong Lin,[b] Tianshu Yang,[a] Lulu Zhang,[a] Qingyi Liu,[b] Chun Zhang *[a] and Fengyu Qian[a]

Hydrotalcite intercalated nanohybrid has served as a vital phosphorescent photosensitizer owing to remarkable $^1O_2$ quantum yield and high cell mortality performance. However, it is rather difficult for potential large or complex guest phosphors to directly intercalate into the hydrotalcite gallery. Hence, it is necessary to regulate the interlayer microenvironment of hydrotalcites firstly for outstanding photosensitive properties. Herein, two isomers, 5,5′BDA and 4,4′BDA, with distinctive dual coordinative features were selected to modify the layer microenvironment of the LGdH gallery and induce the introduction of prospective $Gd(HPhN)_3$ phosphorescent complexes into hydrotalcite through two different coordination effects successively. A LGdH-BDA-$Gd(HPhN)_3$ intercalated nanohybrid phosphorescent photosensitizer was successfully obtained. The results indicated that the more efficient improvement was observed from 5,5′BDA due to offering a more spacious and stable space. Specifically, LGdH-5,5′BDA-$Gd(HPhN)_3$ showed significantly better room temperature phosphorescence properties than LGdH-4,4′BDA-$Gd(HPhN)_3$, whose lifetime was nearly 15 times longer than the latter. Additionally, the LGdH-5,5′BDA-$Gd(HPhN)_3$ system displayed superior singlet oxygen generation *in vitro* under 460 nm irradiation (the quantum yield $\Phi = 0.48$) and outstanding photodynamic therapy performance in tumor cells. LGdH presented more remarkable enhancement performance on the RTP properties of the luminescent molecules. This work provides a novel platform for designing a high-performance hydrotalcite intercalated nanohybrid phosphorescent photosensitizer through coordination induction to regulate the layer microenvironment.

Received 26th October 2023
Accepted 2nd February 2024

DOI: 10.1039/d3ra07310f

rsc.li/rsc-advances

1 Introduction

Photosensitizer, as the core part of photodynamic therapy technology, has garnered considerable attention owing to their high-efficiency $^1O_2$ generation from surrounding $^3O_2$ under light irradiation.[1,2] It is well known that the majority of photosensitizers are based on phosphorescent emission. However, phosphorescence emission is a spin-forbidden radiative decay process severely disturbed by oxygen and temperature.[3] Fortunately, tremendous efforts have been made to explore two strategies to achieve room temperature phosphorescence (RTP). One is to increase intersystem crossing by introducing heavy atoms or heteroatoms (such as carbonyl, N, O, *etc.*) into organic phosphors;[4] the other is to suppress their nonradiative decay through crystallizing, encapsulating in a solid rigid matrix (such as polymers, hydrotalcites, silicones, polyelectrolytes, sol–gels, MOFs, *etc.*) or being assembled into supramolecular systems to limit molecular motion.[5,6]

Among the myriad of matrixes, layered double hydroxides (LDHs, hydrotalcites) are widely selected as a two-dimensional host matrix to construct multicolor host–guest luminescent materials.[7–9] Hydrotalcites possesses the following advantages: (1) the sheet-like structure is easily exfoliated to a monolithic sheet, benefiting for the formation of RTP light-emitting films; (2) the rigid laminate can provide a nano-space confinement effect for guest phosphorescent molecules, and efficiently suppress their motion and boost luminous features; (3) positively charged property can greatly promote the oriented arrangement of guest molecules through electrostatic interaction. Orderly arrangement not only intensifies the interaction between host matrix and guest molecules, but also effectively avoids luminescence quenching caused by agglomeration and improves the photostability as well as thermostability;[10] (4) excellent biocompatibility. When all divalent and trivalent metal ions in the hydrotalcite laminate are replaced by trivalent rare earth ions, layered rare-earth hydroxides (LRH) is

[a]*College of Chemistry and Chemical Engineering, Lanzhou Jiaotong University, Lanzhou 730070, P. R. China. E-mail: zhaozl_521@163.com; zh-chun@163.com*
[b]*State Key Laboratory of Applied Organic Chemistry, Key Laboratory of Nonferrous Metal Chemistry and Resources Utilization of Gansu Province, College of Chemistry and Chemical Engineering, Lanzhou University, Lanzhou 730000, P. R. China*

† Electronic supplementary information (ESI) available. See DOI: https://doi.org/10.1039/D3RA07310F

obtained.[11,12] Besides the variable composition and rich intercalation chemical behaviors of ordinary LDH, LRH also possesses the unique coordination and luminescence properties of rare earth ions, endowing it with potential functional photosensitizer application.[13] Tang *et al.* has found that the intercalation of organic ligand sensitizers into the LRH host laminates can construct tandem energy transfer channels and significantly boost the luminescent properties.[14,15] Similarly, the numerous distinctive luminescent materials were designed with LRH gallery through host–guest tactics.[16–18] However, the reported phosphorescent materials based on LRH host matrix were only limited to various simple structural luminescent molecules. It is very difficult for large or complex prospective phosphors to settle in LRH gallery and acquire an admirable RTP emission. Feasible tactics confronting this challenge is to regulate the interlayer microenvironment of hydrotalcites firstly, and then provide a desired nano-confined effect to realized RTP emission and photosensitizer application.

In this work, two isomers 5,5′BDA and 4,4′BDA with distinctive dual coordinative properties were selected, for the one thing to adjust layer microenvironment of LGdH gallery through the coordination between the carboxylate group in BDA and LRH host matrix firstly, for the other thing to induce potential $Gd(HPhN)_3$ phosphor (HPhN = L) into hydrotalcite by the other coordination effect between two N atoms in BDA and gadolinium complex. Finally, LGdH gallery provided an admirable nano-confined effect on $Gd(HPhN)_3$ complex and the LGdH-BDA-GdL_3 nanohybrid phosphorescent photosensitizers were acquired. The results displayed better tuning effect was present in 5,5′BDA. Specifically, the phosphorescent decay lifetime of LGdH-5,5′BDA-GdL_3 at room temperature was nearly 15 folds longer than LGdH-4,4′BDA-GdL_3. Furthermore, the LGdH-5,5′BDA-GdL_3 system showed significant singlet oxygen $^1O_2$ generation *in vitro* at 460 nm irradiation (Φ = 0.48) and outstanding photodynamic therapy performance in tumor cells. Owing to the heavy atom effect of Gd, the RTP properties of luminescent complex were enhanced more considerably resulted by LGdH than LEuH. This work presented here not only provides a novel platform for designing high-performance phosphorescent photosensitizer with LRH, but also offers some guidelines for adjusting layer microenvironment through coordination (Scheme 1).

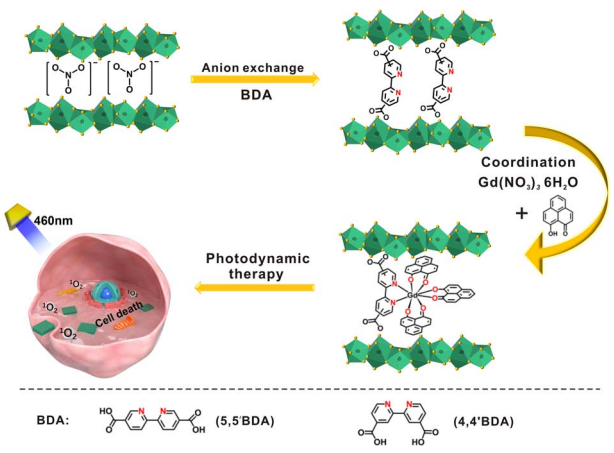

Scheme 1 Schematic of the formation process and photodynamic therapy application of LGdH-BDA-GdL_3 phosphorescent photosensitizer.

2 Experimental section

2.1 Materials and instruments

Gadolinium nitrate [$Gd(NO_3)_3 \cdot 6H_2O$], 2,2′-bipyridine-4,4′-dicarboxylic acid (4,4′ BDA), 2,2′-bipyridine-5,5′-dicarboxylic acid (5,5′ BDA), 2,2,6,6-tetramethylpiperidine (TEMP), 1,3-diphenylisobenzofuran (DPBF), 2-methoxynaphthalene cinnamoyl chloride, 2,2′-bipyridine (Bpy), 2,2′-bipyridine-5,5′-dicarboxylate (DBDO) were obtained from Tianjin Heowns Biochem LLC (China). Magnesium sulfate ($MgSO_4$), potassium hydroxide (KOH) and potassium nitrate (KNO_3) were purchased from Tianjin Damao Chemical Reagent Co., Ltd (China). Aluminum chloride ($AlCl_3$), sodium hydroxide (NaOH), potassium chloride (KCl), hydrochloric acid (HCl), ammonium hydroxide ($NH_3 \cdot H_2O$) and 1,2-dichloroethane (CH_2ClCH_2Cl) were bought from Chengdu Kelong Chemical Co., Ltd (China). 3-((4,5-Dimethylthiazol-yl)-2,5-dimethylthiazol-2-yl)2,5-diphenyltetrazolium bromide (MTT), calcein-AM, propidium iodide (PI) and 2′,7′-dichlorofluorescent yellow diacetate (DCFH-DA) were provided by Singma-Aldrich corporation. Fetal bovine serum (FBS) and Eagle's medium (DMEM) were supplied by Biosharp Life Science (Guangzhou, China). *N*,*N*-Dimethylformamide (DMF), anhydrous ethanol (EtOH), acetonitrile (CH_3CN), dichloromethane (CH_2Cl_2) and other present solvents in this work were offered by Lianlong Bohua Medicine Chemical Co., Ltd (China). The whole materials were analytical reagent (AR) grade and utilized without the further purification.

Power X-ray diffraction (PXRD) patterns were carried out on Rigaku-Dmax 2400 diffractometer with 2θ ranging from 3.5 to 80° and a 5° min^{-1} scanning rate. UV-vis absorption spectra were obtained by a Cary 5000 Spectrometer. The ^1H NMR spectra were recorded on a Bruker 400 MHz spectrometer in $CDCl_3$ solvent. Inductively coupled plasma-atomic (ICP) emission spectroscopy was determined with an IRIS Advantage ER/S spectrophotometer. Fourier transform infrared (FTIR) spectrometry was collected on a Nicolet 360 FTIR spectrometer by a KBr pellet technique with the range from 4000 to 400 cm^{-1} wavenumber. Scanning electron microscopy (SEM) images were conducted with a S-Hitachi 3400N (200 kV). Electrospray ionization mass spectrometry (ESI-MS) spectra were performed on a gas chromatograph/mass spectrometer (HP 5988A). Elemental analysis was analyzed by an Elementar Vario EL analyzer. The phosphorescence spectra, decay lifetime and entire quantum yields of the species were conducted on Hitachi F-45 spectrophotometer. The steady-state luminescence spectra properties were carried out on Edinburgh FSL920 instrument with 450 W Xe arc lamp serving as an excitation source. The Brunauer–Emmett–Teller (BET) specific surface areas were measured by N_2 adsorption–desorption technology on an ASAP 2020 V4.00 (V4.00 H) instrument.

2.2 Fabrication of the layered rare-earth hydroxides (LRH, R = Gd, Eu)

LGdH was synthesized referring to a previously reported literature.[14] A certain amount of KNO_3 and $Gd(NO_3)_3\cdot 6H_2O$ were dissolved in deionized water. KOH solution was added dropwise until the above solution gradually turned cloudy with continuous stirring. Subsequently, the suspension was transferred into a 50 mL Teflon-lined stainless-steel autoclave after 15 min stirring. The obtained white precipitation was centrifuged and washed with deionized water for several times, then dried overnight in a vacuum oven at 50 °C. The ICP and element analysis results indicated the chemical formula of sample: $Gd_2(OH)_{4.74}(NO_3)_{0.86}(CO_3)_{0.45}\cdot 1.11H_2O$ (found: N 2.445, C 1.105, H 1.403, Gd 63.37. Calc.: N 2.447, C 1.109, H 1.406, Gd 63.45).

LEuH was prepared with the same procedure except $Gd(NO_3)_3\cdot 6H_2O$ replaced by $Eu(NO_3)_3\cdot 6H_2O$. The chemical formula obtained from ICP and element analysis results was: $Eu_2(OH)_{4.74}(NO_3)_{0.91}(CO_3)_{0.25}\cdot 1.37H_2O$ (found: N 2.640, C 0.626, H 1.573, Eu 63.04. Calc.: N 2.645, C 0.630, H 1.570, Eu 62.98).

2.3 Preparation of LRH-5,5′BDA intercalated composite (R = Gd, Eu)

5,5′BDA (132.6 mg, 0.54 mmol) was dispersed in DMF (7 mL). Meanwhile, KOH (60.48 mg, 1.08 mmol) was dissolved in deionized water (5 mL). Then, KOH solution was introduced dropwise into 5,5′BDA suspension at 70 °C. After 15 min stirring, the LRH (120 mg) suspension was added to the above reaction mixture at 50 °C and continued to stirred for another 48 h. Finally, the product was centrifuged, washed and dried at 50 °C overnight in a vacuum oven. The chemical formulas of the product obtained from ICP and element analysis result: $Gd_2(OH)_{4.74}(C_{12}H_6N_2O_4)_{0.55}(NO_3)_{0.064}(CO_3)_{0.85}\cdot 2.50H_2O$ (found: N 2.465, C 13.765, H 2.064, Gd 50.06; calc.: N 2.597, C 14.245, H 2.077, Gd 50.03). $Eu_2(OH)_{4.74}(C_{12}H_6N_2O_4)_{0.51}(NO_3)_{0.070}(CO_3)_{0.72}\cdot 2.23H_2O$ (found: N 2.553, C 13.74, H 2.062, Eu 51.16; calc.: N 2.562, C 13.78, H 2.058, Eu 51.04).

2.4 Preparation of LGdH-4,4′BDA intercalated composite

LGdH (110 mg) powder was dispersed in deionized water (1.5 mL) with 15 min ultrasonic treatment. 4,4′BDA (122 mg, 0.5 mmol) was also dispersed in deionized water (2.0 mL), and adjusted pH ≈ 7 *via* adding dropwise NaOH (0.5 mol L^{-1}). Then, LGdH suspension was added to the reaction mixture. After 10 min stirring, the mixture was transferred into a 50 mL Teflon-lined stainless-steel autoclave and continuously reacted at 120 °C for 18 h. The product was treated with centrifugation, washing and drying overnight at 50 °C processes. The chemical formulas of the sample acquired by ICP and element analysis were following: LGdH-4,4′BDA, $Gd_2(OH)_{4.74}(C_{12}H_6N_2O_4)_{0.57}(NO_3)_{0.035}(CO_3)_{0.53}\cdot 1.81H_2O$ (found: N 2.615, C 14.82, H 1.967, Gd 52.38; calc.: N 2.745, C 14.77, H 1.966, Gd 52.41).

2.5 Synthesis of $Gd(HPhN)_3$ (ref. 19)

HPhN was previously synthesized by our group referring to literature.[20] Yellow HPhN (78.4 mg, 0.4 mmol) powder was dissolved in ethanol (7 mL) including 100 μL of 25% aqueous ammonium hydroxide. $Gd(NO_3)_3\cdot 6H_2O$ (59.6 mg, 0.133 mmol) was dissolved in 1 mL deionized water and ethanol mixture (1 : 4 v/v). The solution was added drop by drop to the hot HPhN solution (70 °C), and continued to stir for 5–20 min until an obvious red shift of the UV-vis absorption peaks in the visible region compared with HPhN was observed. The dark yellow product was obtained by mean of centrifuging and washing with water and methanol. The crude precipitate was used no further purification. HRMS (ESI-MS): $[M + H]^+$ *m*/*z*, calc.: 744.0579, found: 744.1014; elemental analysis $C_{39}H_{21}GdO_6$ (%): calc.: C 63.06, H 2.85, Gd 21.17; found: C 63.72, H 2.53, Gd 20.69.

2.6 Preparation of LRH-5,5′BDA-$Gd(HPhN)_3$ (LRH-5,5′BDA-GdL_3 for simplification, R = Gd, Eu)

LRH-5,5′BDA (50 mg) was uniformly discrete in acetonitrile (5.5 mL) under 30 min sonication treatment. $Gd(NO_3)_3\cdot 6H_2O$ (13.54 mg, 0.03 mmol) was in advance dissolved in acetonitrile (1.0 mL) and then introduced drop by drop to the mentioned LRH-5,5′BDA suspension. The mixture was reacted at 60 °C for 3 h. Meanwhile, HPhN (17.6 mg, 0.09 mmol) was also dissolved in acetonitrile (4.0 mL) with ultrasonic treatment, and deprotonated with ammonia (45 μL, 25%). Subsequently, the HPhN solution was added to the original reaction system and continued to react 48 h. The final product was treated with centrifugation, washing with acetonitrile for three times and drying at 40 °C overnight to obtain a yellow sample.

2.7 Preparation of LGdH-4,4′BDA-GdL_3 and LGdH-5,5′BDA-L

LGdH-4,4′BDA-GdL_3: the fabrication process is similar to LGdH-5,5′BDA-GdL_3, except that the mixture of LGdH-4,4′BDA and $Gd(NO_3)_3\cdot 6H_2O$ was react at 60 °C for 5 h and then 48 h.

LGdH-5,5′BDA-L: the preparation procedure is also approximate to LGdH-5,5′BDA-GdL_3 except for no $Gd(NO_3)_3\cdot 6H_2O$ introduction.

2.8 Synthesis of $Gd(Bpy)(HPhN)_3$ and $Gd(DEBO)(HPhN)_3$ control complexes[19]

The 2,2′-bipyridine (15.6 mg, 0.1 mmol) or diethyl 2,2′-bipyridine-5,5′-dicarboxylate (30.0 mg, 0.1 mmol) was dissolved in toluene (5 mL), and then added drop by drop to the hot dispersion of $Gd(HPhN)_3$ (74.3 mg, 0.1 mmol) in toluene (5 mL). The mixture was continued to heat for 1–2 h. The resulted solution was rapidly cooled to room temperature and centrifuged to acquire the desired complex. Gd $Gd(Bpy)(HPhN)_3\cdot 1.70C_7H_8$, yield: 34.0 mg (35.5%). ESI-MS ($[M\text{-}1HPhN]^+$): *m*/*z* 876.2362; elemental analysis for $C_{51}H_{35}GdN_2O_6\cdot 1.70C_7H_8$ (%): calc.: C 69.73, H 3.22, N 2.58, Gd 14.46; found: C 69.89, H 3.34, N 2.41, Gd 14.35. $Gd(Dbdo)(HPhN)_3\cdot 1.53C_7H_8$, yield: 34.0 mg (35.5%). ESI-MS ($[M\text{-}1HPhN]^+$): *m*/*z* 1004.1801; elemental analysis for $C_{56}H_{40}GdN_2O_{10}\cdot 1.53C_7H_8$ (%): calc.: C 66.77, H 3.34, N 2.33, Gd 13.09; found: C 66.70, H3.41, N 2.23, Gd 13.13.

2.9 Phosphorescence properties determination

Low temperature (77 K) phosphorescent spectra were acquired through an NMR tube laid in a quartz-walled Dewar flask filled with liquid nitrogen. RTP spectra and decay lifetimes were measured using the identical instrument without liquid nitrogen. The luminescence experiments under different oxygen concentrations were carried out by bubbling various volume ratios of N_2 and O_2 gaseous mixtures for 5–6 min. Overall quantum yields were determined through an absolute method with an integrating sphere (150 mm diameter, $BaSO_4$ coating).

2.10 ROS measurement

ROS yields from LGdH-BDA-GdL_3 were evaluated by four ways: $^1O_2$ emission spectra, EPR spectra, DPBF technique and DCFH method. Those detailed processes were described as follows:

EPR spectra: 2,2,6,6-tetramethylpiperidine (TEMP) was served as a trapping agent. The samples were respectively dispersed in deionized water (1.0 mg mL^{-1}) containing a certain amount of TEMP (120 μM), and irradiated with 460 nm LED lamp (20 W) for 10 min, then determined with EPR instrument.

DPBF technique: the samples were dispersed in the solution DPBF in anhydrous ethanol (78 μM, 20 mL), the concentration was about 25 μg mL^{-1}. Then, the UV-vis absorption spectrum of DPBF was continuously tested when the suspension was irradiated with 460 nm LED lamp (20 W) for 10 s every time. Observe the absorbance change of the absorption peak of DPBF around 426 nm with the illumination time. Other samples to be tested were kept in the dark.

DCFH approach: the sample was dispersed in DMF containing a certain amount of DCFH (5.2 μM), the concentration is about 20 μg mL^{-1}. The suspension was intermittently irradiated with 460 nm LED lamp (20 W) for 2 min each time, then measured the fluorescence spectrum of DCFH (λ_{ex} = 488 nm), and observed the intensity of the fluorescence peak at 525 nm with the irradiation time.

3 Results and discussion

3.1 Structural characterization of LRH precursor

The hydrothermal technique reported in numerous literatures was adopted in this work to prepare the LGdH precursor. In the method, the initial concentration of rare earth ions (c), stirring time (t_1), hydrothermal temperature (T) as well as hydrothermal time (t_2) acted as the crucial factors affecting on the morphology and size of hydrotalcite sheets.[21] LGdH species in previous studies were regular hexagonal lamellar structure in the micrometer scale.[21] Nevertheless, it was well accepted that more regular sample with smaller size (<200 nm) are favored for exploitation of photosensitizer and photodynamic therapy application. Therefore, an orthogonal test was designed to investigate the optimum process conditions, and displayed in the Table S1.† The optimum preparation parameters from the test were as follows: 0.05 mol L^{-1} (the concentration of Gd^{3+} ion), 5 min (stirring time), 120 °C (hydrothermal temperature), and 36 h (hydrothermal time). The LGdH sample obtained under the preferred plan was characterized at length in Fig. S1.† It was found that the LGdH sample was present in the form of a quasi-tetragonal plate-like nanosheet, with the average side length around 109 nm (Fig. S1a and b†), and the thickness about 11 nm (Fig. S1c†). The layered structure was clear and distinct (Fig. S1c†). According to the crystal structure data of LRH intercalates (CCDC-604276 and -604277), the single LRH sheet was about 0.65 nm thickness.[22] Endowing a potential outstanding luminant property with the gallery. The molecular formula of LGdH determined by ICP and elemental analysis was $Gd_2(OH)_{4.74}(NO_3)_{0.86}(CO_3)_{0.45}\cdot 1.11H_2O$. Fig. S1d† shows a series of (002), (004) and (006) diffraction peaks, which were served as a characteristic layered rare earth hydroxide phase with a basal spacing of 0.83 nm.[23] In the meantime, a relatively weaker (220), non-(00l) diffraction peak, was also in sight, displaying a typical ordered, two-dimensional lamellar stacking structure. Meanwhile, the optimum preparation parameters for LEuH were 0.05 mol L^{-1}, 5 min, 90 °C and 24 h. The molecular formula was $Eu_2(OH)_{4.74}(C_{12}H_6N_2O_4)_{0.51}(NO_3)_{0.070}(CO_3)_{0.72}\cdot 2.23H_2O$. Compared to LGdH, LEuH was present less uniform morphology with the majority of nanosheets and the minority of long rods (Fig. S2a and b†). However, the crystalline structure was similar as LGdH, and the diffraction peaks were located at 10.08°, 19.98°, 28.28° and 30.34°.

3.2 Structural analysis of intercalated nanohybrids

Two isomers 4,4′BDA and 5,5′BDA were successfully intercalated into LGdH gallery. The molecule formula of these compounds obtained from ICP and elemental analysis were $Gd_2(OH)_{4.74}(C_{12}H_6N_2O_4)_{0.55}(NO_3)_{0.064}(CO_3)_{0.85}\cdot 2.50H_2O$ (LGdH-5,5′BDA) and $Gd_2(OH)_{4.74}(C_{12}H_6N_2O_4)_{0.57}(NO_3)_{0.035}(CO_3)_{0.53}\cdot 1.81H_2O$ (LGdH-4,4′BDA), respectively. It can be seen that the amount of two BDA ions fixed in LGdH was close to each other. The initial nitrate ions are mostly replaced by BDA ions. Ions exchanging has brought about great changes in the morphology and shape of LGdH host layer. Original lamellar has converted into nanoparticles with no obvious size change (around 110 nm). Compared with LGdH-4,4′BDA, LGdH-5,5′BDA nanohybrid was present more uniformly without evident aggregation (Fig. 1a and b). Successful ions exchanging in LGdH gallery is also verified by PXRD patterns result (Fig. 1c) owing to the apparent shifting of systemic (00l) reflections of LGdH-BDA to lower diffraction angles. Taking (002) diffraction peak for example, it shifts from 10.82° to 5.48° and 5.96° for LGdH-5,5′BDA and LGdH-4,4′BDA, respectively, corresponding the basal spacing expanded from 0.83 nm to 1.64 nm, 1.50 nm (Table S2†). Related to LGdH-BDA, the (00l) reflections of LGdH-BDA-GdL_3 shifts marginally to lower diffraction angles, and the basal spacing narrowed to 1.58 nm for 5,5′BDA, and nearly no change for 4,4′BDA. Additionally, the basal spacing of the asymmetric (220) reflections change from 0.33 nm to 0.32 nm before and after intercalation of BDA, revealing that a certain change exhibited in the host laminate, which is resulted from the coordination between the BDA guest molecules and rare earth cations in the host laminate.[15] Furthermore, the relative intensity of (002) and (004) reflection peaks vary distinctly after introduction of BDA with respect to the (220) reflecxtions,

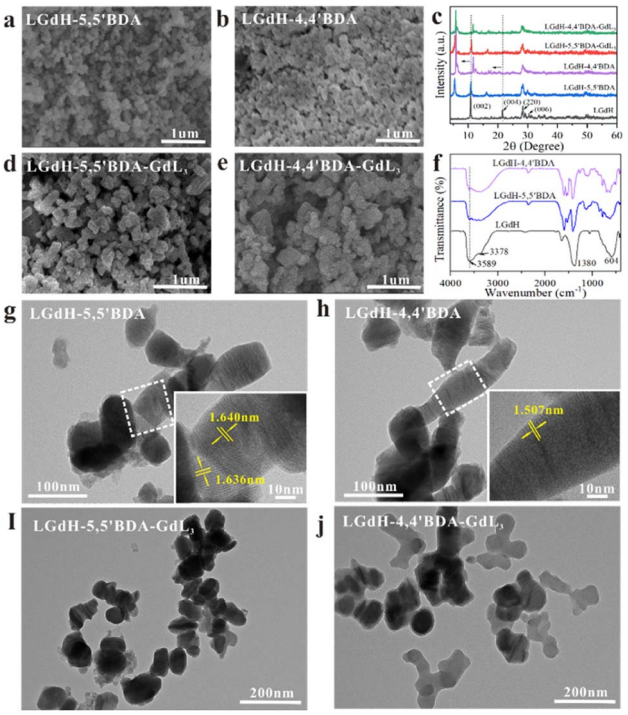

Fig. 1 SEM images of (a) LGdH-5,5′BDA, (b) LGdH-4,4′BDA, (d) LGdH-5,5′BDA-GdL_3 and (e) LGdH-4,4′BDA-GdL_3; (c) PXRD patterns of LGdH and above mentioned four intercalated nanohybrids; (f) FTIR spectra of LGdH, LGdH-5,5′BDA and LGdH-4,4′BDA, TEM images of four intercalated nanohybrids (g–j).

indicating the regularity degree became less ordered or the thickness of LGdH platelets declined along the *c*-axis.[15] The PXRD pattern is good consistent with previous reports.[14,24–26] The layer morphology of LRH is clearly present in Fig. 1g and h, and the basal spacings of LGdH-BDA measured in TEM images are well coincident with the values calculated from PXRD result. Additionally, compared to bare LGdH-5,5′BDA-GdL_3, LGdH-4,4′BDA-GdL_3 seems to be coated with an unknown substance (Fig. 1i and j).

The FTIR spectra of LGdH, LGdH-5,5′BDA and LGdH-4,4′BDA species are displayed in Fig. 1f. Intense broad bands centered at 3589 cm^{-1} and 3378 cm^{-1} are ascribe to the stretching mode of the hydroxyl group from both rare earth hydroxide layers and the interlayer water molecules. Simultaneously, the absorption peak assigned to the bending vibration of water molecules is appeared around 1634 cm^{-1}. The strong band at 1380 cm^{-1} corresponds to the ν3 mode of the NO_3^- species.[15] The strong broad band at 604 cm^{-1} is observed, which is attributed to the stretching vibration of Gd–O in hydroxide layer. After exchanging with BDA, the absorption peak at 3378 cm^{-1} is red-shifted to 3448 cm^{-1} and widen, verifying there is a hydrogen interaction between BDA anions and the host LGdH matrix, which served as an energy transfer channel to facilitate the sensitization of rare earth ions in host gallery by interlayer organic ligands.[27] The peak of the retained NO_3^- anions at 1380 cm^{-1} is overlapped with 1411 cm^{-1}. For investigation, detailed comparison of the FTIR spectra of BDA, LGdH

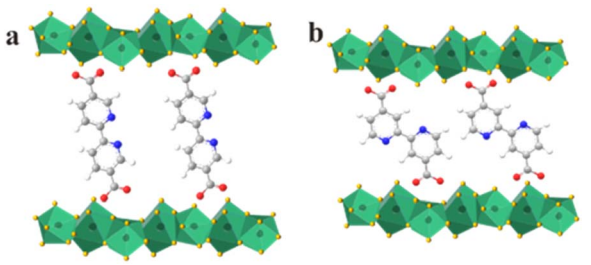

Fig. 2 The proposed arrangement mode of (a) 5,5′BDA and (b) 4,4′BDA in LGdH gallery.

and LGdH-BDA, HPhN (L) ligand, GdL_3 and LGdH-BDA-GdL_3 samples are shown in Fig. S3 and S4.† The characteristic asymmetric and symmetric stretching vibrations of the $-COO^-$ group in 5,5′BDA are present at 1689 cm^{-1} (–C=O), 1424 cm^{-1} and 1307 cm^{-1} (–C–O), which shifts to 1658 cm^{-1} along with the intensity sharply decreased, 1411 cm^{-1}, and 1307 cm^{-1} without transmittance in LGdH-5,5′BDA (Fig. S3a†). Similar to 5,5′BDA, the typical vibrations of the $-COO^-$ group in LGdH-4,4′BDA are shifted from 1715 cm^{-1} to 1658 cm^{-1}, 1460 cm^{-1} to 1417 cm^{-1}, 1297 cm^{-1} to 1261 cm^{-1} as well as intensity decrease (Fig. S4a†). Peak shifts and intensity apparent variations demonstrate that both two O atoms (O=C–O–) are probably to participate in the coordination with the host matrix, which induced to the orientation arrangement of BDA molecular in LGdH gallery. The proposed arrangement of BDA in host LGdH is displayed in Fig. 2. In Fig. S3b,† besides $\nu_{(O=CO-)}$ of 5,5′BDA, the symmetric stretching vibrations of the –C=O group in HPhN (1632 to 1621 cm^{-1}) was also observed in the FTIR spectra of LGdH-5,5′BDA-GdL_3, accompanying with 1589 cm^{-1} (overlapping with –C=N in pyridine ring), 1525 cm^{-1}, and 1420 cm^{-1} (characteristic –C=C stretching vibrations peaks of aromatic ring in GdL_3), verifying that the analogous rare earth complexe existed in the nanohybrid. It is concluded that the binding vibrations of ligands in nanohybrid may be the N–N atoms of the BDA anion to coordinate with Gd(III) ions in GdL_3 which induces the intercalation of complex. Additionally, three L ligands provide their six O atoms to simultaneously interact with Gd(III) ions to satisfy coordination saturation of rare earth ions.[15] However, the characteristic vibrations of GdL_3 cannot be well shown in LGdH-4,4′BDA-GdL_3 nanohybrids.

In order to investigate the entrance of GdL_3 complex into LGdH-BDA, elemental analysis result, N_2 adsorption–desorption experiment and UV-vis spectra of series of nanohybrids were performed. Theoretically, the mole ration of C/N will gradually increase accompanying with in intercalation of rare earth complex due to there is no N element in complex. Actually, the *n* (C/N) increased from 6.51 to 9.11, and 6.60 to 13.5 for LGdH-5,5′BDA-GdL_3 and LGdH-4,4′BDA-GdL_3 (Table 1), respectively. Related to LGdH-5,5′BDA, the Brunauer–Emmett–Teller (BET) specific surface of LGdH-5,5′BDA-GdL_3 decreased from 26.2 to 10.2 $m^2\ g^{-1}$. Ridiculously, a slight enhancement displays in the BET specific surface value of LGdH-4,4′BDA-GdL_3 (19.0 to 23.0 $m^2\ g^{-1}$). From the UV-vis spectra result in Fig. S5,† it is also found the absorbance spectra of GdL_3 are

Table 1 Elemental analysis results of various nanohybrids

Sample	N (%)	C (%)	H (%)	Gd (%)	*n* (C/N)
LGdH-5,5′BDA	2.47	13.77	2.06	50.06	6.51
LGdH-4,4′BDA	2.62	14.82	1.97	52.38	6.60
LGdH-5,5′BDA-GdL_3	2.78	21.71	2.26	46.05	9.11
LGdH-4,4′BDA-GdL_3	2.53	29.42	2.82	50.06	13.50

evidently present in LGdH-BDA-GdL_3 species, but the spectrum of BDA (290–320 nm) is almost disappeared in LGdH-4,4′BDA-GdL_3. Using the above insights, it is concluded that the successful intercalation of potential rare earth complex phosphor is only present in LGdH-5,5′BDA system owing to its more spacious layer environment (1.64 nm basal spacing), but failed for LGdH-4,4′BDA (1.50 nm basal spacing). It is very possible for HPhN ligand to absorb on the surface of LGdH host matrix and coordinate with Gd atom in LGdH-4,4′BDA. Combined with TEM images LGdH-4,4′BDA-GdL_3 (Fig. 1j), it is certain that the substance coated on the surface is HPhN. Simultaneously, a small amount of 4,4′BDA molecules shed from the LGdH because of unstable coordination with the host matrix, which is well agreed with the previous FTIR discussion. Based on the above observation, it comes to a conclusion that BDA ions play a pivotal role in regulating the microenvironment of the LGdH gallery, of which 5,5′BDA provides more spacious space than 4,4′BDA and benefits for the subsequent introduction of GdL_3 complex and formation of high-performance nanohybrid photosensitizer.

3.3 Phosphorescence behave

To evaluate the enhancement effect of LGdH-BDA on GdL_3 complex, the comparison of RTP property of GdL_3 and LGdH-BDA-GdL_3 is shown in Fig. 3. The free GdL_3 almost has no RTP signal, which is consistent with previous studies.[28,29] The coordination with rare earth ion only contributes to improve the low-temperature (77 K) phosphorescence property and reduce the difference of energy level between HOMO and LUMO of HPhN ligand (namely, an obvious red-shifting in the emission spectrum of complex was observed) (Fig. S6†). The characteristic RTP emission wavelengths of LGdH-5,5′BDA-GdL_3 and LGdH-4,4′BDA-GdL_3 nanohybrids are both present around 560 nm, which is close to the reported $Gd(HPhN)_3$phen, $Gd(HPhN)_3$dpp and $Gd(HPhN)_3$ DDXPO complexes.[19] However, the luminescence intensity of LGdH-5,5′BDA-GdL_3 is nearly 8 times more than that of LGdH-4,4′BDA-GdL_3. The values of luminescence decays corresponded to the LGdH-BDA-GdL_3 solid samples (Fig. S7†) are coincident with the single exponent, 1294 μs for LGdH-5,5′BDA-GdL_3, and 92 μs for LGdH-4,4′BDA-GdL_3 (Fig. 3b). The former is two orders of magnitude longer than the latter. The luminescence quantum efficiency $\Phi_{overall}$ was surveyed with an integrating sphere apparatus. The absolute quantum yields of LGdH-5,5′BDA-GdL_3 and LGdH-4,4′BDA-GdL_3 are 0.79% and 0.61%, respectively. The phosphorescence decay lifetime of the unintercalated GdL_3 is less than 1 μs, and the absolute quantum yield is too low to be detected. Apparently, LGdH-5,5′BDA-GdL_3 exhibits more highly-performing RTP property, indicating that the intercalation effect into LGdH-BDA is more efficient than the absorbance on the surface of LGdH gallery in enhancement of RTP property of rare complex phosphor.

To further illustrate the LGdH gallery nano-confined effect on the RTP property of GdL_3 complex. Free complex was also synthesized to act as control group. Nevertheless, two carboxyl groups in BDA will preferentially coordinate with rare earth ions, so it was rather difficult to gain the desired $GdBDAL_3$ complex. According to the reported literature,[19] a series of GdL_1L_3 (L_1 = phen, dpp, DDXPO) exhibited the similar photoluminescence behavior. Namely, RTP phenomenon of the GdL_1L_3 mostly relays on GdL_3 group.[19] Consequently, bipyridine (Bpy) and diethyl bipyridyl oxalate (DEBO) were selected to serve as a substitute for BDA and acquire free $Gd(Bpy)L_3$ and $Gd(DEBO)L_3$ complexes. The phosphorescence spectra at room temperature of LGdH-5,5′BDA-GdL_3, $Gd(Bpy)L_3$ and $Gd(DEBO)L_3$ were displayed in Fig. 4a. It is found that the luminescence intensity of these complexes is close to each other, whose phosphorescence decay lifetime values are 4.5 μs and 6.8 μs, respectively. However, LGdH-5,5′BDA-GdL_3 intercalated nanohybrid achieved nearly 30 folds higher intensity and almost 190 folds longer decay lifetime than that of free complexes, indicating that the nano-confined effect of LGdH gallery plays a key role in boosting of RTP property. In previous discussion, it is found that a certain amount of HPhN adsorbed and coordinated with rare earth ion on the LGdH host. To investigate the

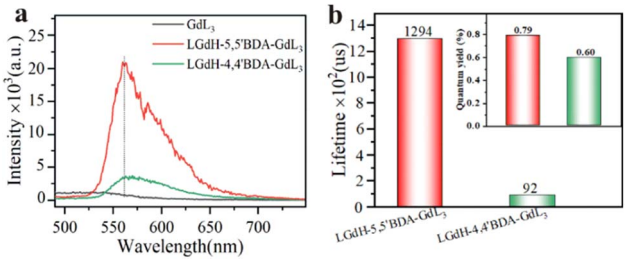

Fig. 3 RTP property of GdL_3, LGdH-5,5′BDA-GdL_3 and LGdH-4,4′BDA-GdL_3, (a) intensity (gate 100 μs, λ_{ex} = 460 nm) and (b) lifetime, inner: quantum yield (560 nm, λ_{ex} = 460 nm).

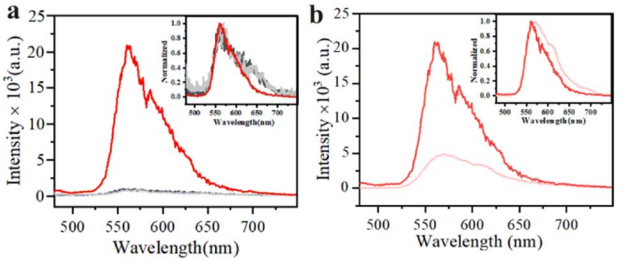

Fig. 4 The phosphorescence spectra of (a) LGdH-5,5′BDA-GdL_3 (red line, 0.5g mL^{-1}), $Gd(Bpy)L_3$ (light gray line, 5.0 × 10^{-5} mol L^{-1}) and $Gd(DEBO)L_3$ (dark gray line, 5.0 × 10^{-5} mol L^{-1}), (b) LGdH-5,5′BDA-GdL_3 and LGdH-5,5′BDA-L (light red line, 0.5 g mL^{-1}) (gate 100 μs, λ_{ex} = 460 nm, room temperature, C_2H_5OH solvent).

influence of absorbed coordination on the RTP property, another control group LGdH-5,5′BDA-L was prepared and studied, whose RTP behavior is seen in Fig. 4b. Under the same concentration and test condition, the luminescence intensity of LGdH-5,5′BDA-L is a quarter of LGdH-5,5′BDA-GdL_3 and close to LGdH-4,4′BDA-GdL_3, but the decay lifetime is far shorter than that of the desired nanohybrid, the value is merely 3.53 μs. Based on the above comparison, it draws a conclusion that the high RTP performance of nanohybrids mostly arises from the coordination of rare earth ions and the nano-confinement effect of LGdH-5,5′BDA. Furthermore, the BDA molecules almost have no absorbance at 460 nm (Fig. S8†), suggesting there is nearly no energy resonance transfer between BDA and L ligand through central Gd(III) ion at irradiation. Meanwhile, the photostability of LGdH-5,5′BDA-GdL_3 in water is significantly superior to LGdH-4,4′BDA-GdL_3 (Fig. S9†).

3.4 O_2-sensitivity

The O_2-sensitivity of LGdH-5,5′BDA-GdL_3 suspension with the optimal RTP performance in water was tested, as seen in Fig. S10.† Both the phosphorescence emission intensity and decay lifetime gradually decrease with the increasing of O_2 concentration. Furthermore, it shows good linear relationships between decay lifetime ratio (τ_0/τ) and O_2 concentration. Meanwhile, the profile of the luminescence intensity ratio (I_0/I) with O_2 concentration can also be plotted as a nearly straight line. The experimental survey verifies LGdH-5,5′BDA-GdL_3 possess the significant O_2-sensitive property, and the luminescence intensity is more sensitive to external factors such as O_2 concentration.[27]

3.5 $^1O_2$ production

It is acknowledged accepted that oxygen is converted into singlet state oxygen ($^1O_2$) while phosphorescence emission being quenched by oxygen molecules, thus LGdH-BDA-GdL_3 is employed as a potential phosphorescent photosensitizer. The $^1O_2$ generation ability was evaluated adequately by $^1O_2$ emission spectrum, EPR technique, DPBF UV-vis absorption and DCFH fluorescence four methods, as displayed in Fig. 5. In general, the $^1O_2$ emission spectrum is located around 1272 nm. Both LGdH-5,5′BDA-GdL_3 and LGdH-4,4′BDA-GdL_3 appear obvious $^1O_2$ emission peaks at the same concentration of water suspension in the air, but the luminescence intensity of LGdH-5,5′BDA-GdL_3 is apparently higher than LGdH-4,4′BDA-GdL_3 (Fig. 5a). Under the same experimental conditions, $^1O_2$ EPR peaks evidently appeared in two LGdH-BDA-GdL_3 nanohybrids, but the intensity comparison result is well consistent with the $^1O_2$ emission peak intensity (LGdH-5,5′BDA-GdL_3 > LGdH-4,4′BDA-GdL_3, Fig. 5b). Due to the absorption peak at 426 nm will gradually decrease encountering with $^1O_2$, so DPBF has termed as a typical $^1O_2$ detection reagent. Under 460 nm irradiation, the absorbance of the control group slightly decreased accompanying with the prolongation of irradiation time. Regarding LGdH-5,5′BDA-GdL_3 and LGdH-4,4′BDA-GdL_3 samples, the more significant decline trends are present in Fig. S11,† and the rate of decline is: LGdH-5,5′BDA-GdL_3 > LGdH-4,4′BDA-GdL_3 (Fig. 5c). Moreover, DCFH will be oxidized

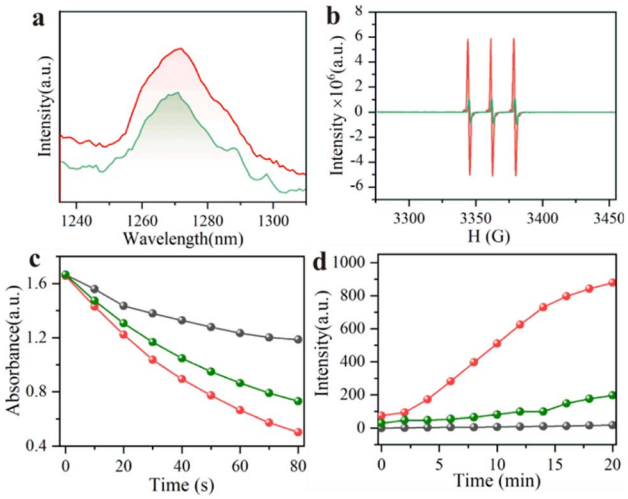

Fig. 5 The $^1O_2$ production of LGdH-5,5′BDA-GdL_3 (red line), LGdH-4,4′BDA-GdL_3 (green line) and contrast blank sample (gray line), (a) emission spectra of $^1O_2$ (room temperature, in air); (b) EPR spectra of $^1O_2$; (c) the absorbance of DPBF at 424 nm with irradiation time; (d) the fluorescence intensity of DCFH at 525 nm with irradiation time. The concentration of samples was 1.0 mg mL^{-1}.

into DCF with luminous green fluorophore at the presence of $^1O_2$, and the intensity of fluorescence enhanced with the increasing of $^1O_2$. As depicted in Fig. S12,† the fluorescence intensity of the control group without sample shows very slight increasement. However, the remarkable enhancement of the intensity is seen in the LGdH-BDA-GdL_3 group under the same experimental conditions, especially for LGdH-5,5′BDA-GdL_3. As shown in Fig. 5d, the increasing rate of the LGdH-5,5′BDA-GdL_3 is also apparently higher than LGdH-4,4′BDA-GdL_3. From the above experimental results, it adequately demonstrates that the $^1O_2$ generation capability of LGdH-5,5′BDA-GdL_3 is superior to LGdH-4,4′BDA-GdL_3. The ability of $^1O_2$ generation result is well agreed with the RTP property of LGdH-BDA-GdL_3 species. Furthermore, the $^1O_2$ quantum yield of LGdH-BDA-GdL_3 samples were also calculated with MB as a reference. The values are 0.48 and 0.36 for LGdH-5,5′BDA-GdL_3 and LGdH-4,4′BDA-GdL_3, respectively. The value is considerably superior to the reported iridium complex photosensitizers Ir-P (ph)$_3$ and Ir-alkyl (0.17 and 0.21, respectively).[29] It lays a solid foundation for the further extensive employment of LGdH-5,5′BDA-GdL_3 nanohybrid photosensitizers.

3.6 Cell experiment results

To assess the photodynamic therapy effect of LGdH-5,5′BDA-GdL_3, cell experiment was carried out on HeLa cells. After incubating cells with LGdH-5,5′BDA-GdL_3 for 4 h, confocal microscopy images shows bright green fluorescence in HeLa cells (Fig. 6a_1, a_2 and a_3), indicating that LGdH-5,5′BDA-GdL_3 nanohybrid has successfully entered cells. The intracellular $^1O_2$ production was investigated using a conventional DCFH-DA indicator. In the presence of $^1O_2$, DCFH is oxidized to produce DCF with bright green fluorescence. As shown in Fig. 6b, HeLa cells loaded with LGdH-5,5′BDA-GdL_3 nanohybrid show weak

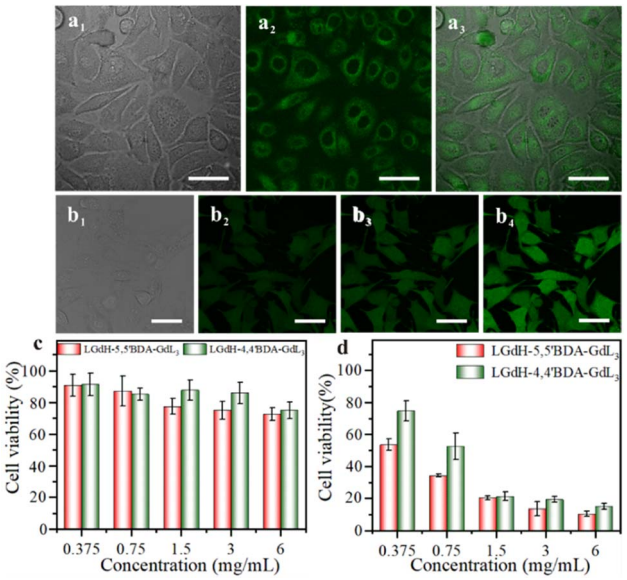

Fig. 6 (a) Confocal microscopic images of HeLa cells cultured with LGdH-5,5′BDA-GdL_3 drug for 4 h, (a_1) bright, (a_2) fluorescence, (a_3) merged; (b) confocal microscopic images of intracellular ROS generation in HeLa cells treated with LGdH-5,5′BDA-GdL_3 irradiated at different times (light source: 460 nm LED lamp, irradiation time: 30 s/time, 5 min interval), (b_1) bright, (b_2) 30 s, (b_3) 60 s, (b_4) 90 s. Scale bar: 40 μm; the cell viability of HeLa cells incubated with different concentrations of LGdH-5,5′BDA-GdL_3 and LGdH-4,4′BDA-GdL_3 (c) without and (d) with 460 nm LED lamp irradiation for 10 min.

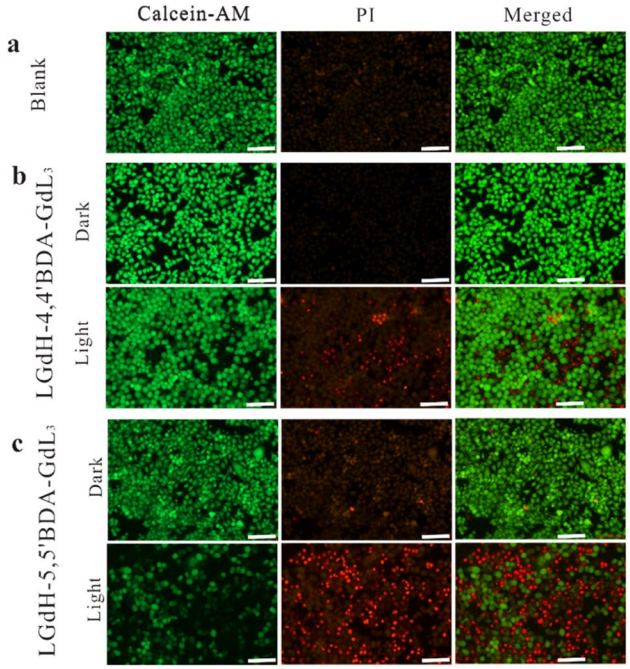

Fig. 7 Live/dead assay of HeLa cells co-stained with calcein-AM/PI after incubation with (a) blank, (b) LGdH-4,4′BDA-GdL_3, (c) LGdH-5,5′BDA-GdL_3 (1.0 mg mL^{-1}) in the dark and under light irradiation (460 nm LED lamp irradiation for 10 min, scale bar 10 μm).

green fluorescence after being irradiated by a 460 nm LED (Fig. 6b_2), and the green fluorescence in the cells became more and more bright along with the prolongation of the irradiation time (Fig. 6b_3 and b_4), suggesting that the prolongation of the irradiation time is beneficial for more $^1O_2$ generation in the cancer cells. The cytotoxicity of LGdH-5,5′BDA-GdL_3 and LGdH-4,4′BDA-GdL_3 on HeLa cells was evaluated by MTT assay. After cells being treated with different concentrations of LGdH-5,5′BDA-GdL_3 or LGdH-4,4′BDA-GdL_3 samples for 24 h, MTT assays were performed. As displayed in Fig. 6c that the high cell viability is evident even at very high concentrations (6.0 mg mL^{-1}) in the absence of irradiation, demonstrating two LGdH-BDA-GdL_3 nanohybrids exhibit low toxicity and good biocompatibility. When irradiated by a 460 nm LED, the viability of cells incubated with the LGdH-5,5′BDA-GdL_3 or LGdH-4,4′BDA-GdL_3 gradually decreases accompanying with the increasing of drug concentration. When the concentration is only 0.375 mg mL^{-1}, the corresponding cell viability are 53.6% and 75.8% for the LGdH-5,5′BDA-GdL_3 or LGdH-4,4′BDA-GdL_3, respectively (Fig. 6d). The concentration is up to 0.75 mg mL^{-1}, the cell viability decreased to 34.3% and 52.6%. With further increase in concentration, the difference between the cell viability incubated with two LGdH-BDA-GdL_3 drugs becomes smaller and smaller, indicating that LGdH-5,5′BDA-GdL_3 present a better photodynamic effect at low concentration. The photodynamic treatment effect of the LGdH-BDA-GdL_3 nanohybrids is well consistent with the *in vitro* $^1O_2$ generation capability. Overall, the LGdH-5,5′BDA-GdL_3 nanohybrids exhibited outstanding photodynamic properties with an IC_{50} value of 0.75 mg mL^{-1}. The photodynamic therapy effect is further verified by the live/dead assay. Herein, the live cells and dead cells were stained with a green fluorescence dye (calcein-AM) and a red fluorescence dye (PI), respectively. As displayed in Fig. 7, compared to the blank group, obvious red fluorescence is observed in the groups treated with LGdH-4,4′BDA-GdL_3 and LGdH-5,5′BDA-GdL_3 drugs under light irradiation, and red fluorescence in the latter is far more than that in the former, indicating the excellent photodynamic therapy effect is present in LGdH-5,5′BDA-GdL_3. The result is well coincident with the MTT results.

3.7 Phosphorescence property of LEuH-5,5′BDA-GdL_3

Taking into account whether a general strategy for layered rare-earth hydroxides to boost the RTP property of GdL_3 complex, the analogue LEuH-5,5′BDA-GdL_3 nanohybrid was also fabricated. Differing from LGdH-5,5′BDA, the minority of LEuH nanosheets are exfoliated into various lamellas in the process of introduction of 5,5′BDA ions (Fig. 8a). Apparent agglomeration is observed in LEuH-5,5′BDA-GdL_3 with further intercalation of gadolinium complex (Fig. 8b). In Fig. 8c, (002) diffraction peak of LEuH-5,5′BDA shifted from 10.01° to 5.54° related to LEuH, so corresponding the basal spacing expanded from 0.83 nm to 1.60 nm, suggesting the successful introduction of 5,5′BDA into LEuH. The RTP spectra of kinds of nanohybrids are shown in Fig. 8d. The typical characteristic peak of Eu (611 nm) is apparently observed in LEuH-5,5′BDA, confirming Eu element in the hydrotalcite host layer is sensitized by 5,5′BDA molecule. Meanwhile, in the spectrum of LEuH-5,5′BDA-GdL_3, the feature RTP peak of GdL_3 located at 560 nm is also present companying the intensity decreasing of 611 nm peak . However, the intensity

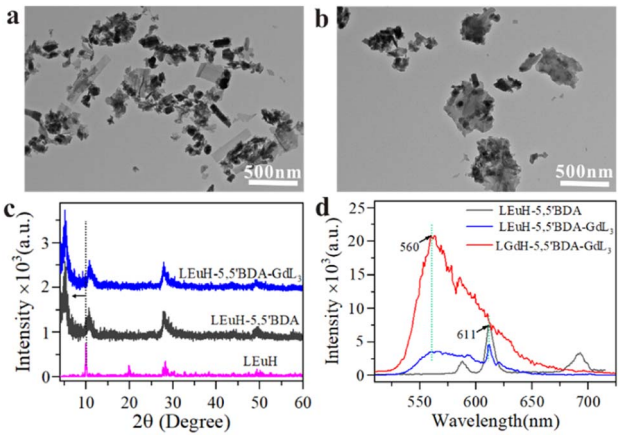

Fig. 8 TEM images of (a) LEuH-5,5′BDA, (b) LEuH-5,5′BDA-GdL_3, (c) PXRD patterns of LEuH and corresponding intercalated nanohybrids, (d) comparison of RTP spectra of LRH-5,5′BDA-GdL_3 (R = Eu, Gd, 0.5 mg mL^{-1}, gate 100 μs, λ_{ex} = 460 nm).

of LEuH-5,5′BDA-GdL_3 at 560 nm is far lower than LGdH-5,5′BDA-GdL_3. It is because that the heavy atom effect of Gd in host matrix is more propitious to the RTP enhancement of luminescent molecules, which are reported in numerous literatures.[28,30]

4 Conclusion

In summary, two isomers 5,5′BDA and 4,4′BDA with unique dual coordination feature were selected in this work to regulate layer microenvironment of LGdH gallery through the coordination between the host LRH matrix and BDA ligand firstly, then induce the intercalation of $Gd(HPhN)_3$ complex phosphor into LRH gallery to acquire an excellent hydroxides-complex intercalated nanohybrids phosphorescent photosensitizer. 5,5′BDA molecular exhibited more effective tuning effect on LGdH gallery than 4,4′BDA due to offering more spacious and stable layer microenvironment in favor for complete entrance of complex. Specifically, LGdH-5,5′BDA-GdL_3 species was present more significant RTP properties and remarkable $^1O_2$ generation capability *in vitro* at 460 nm blue light irradiation (Φ = 0.48) than LGdH-4,4′BDA-GdL_3. Furthermore, it also showed outstanding photodynamic therapy performance in tumor cells. LGdH displayed more remarkable enhancement effect on the RTP property of luminescent molecules due to the heavy atom effect of Gd. This work explores a new platform to construct high-performance phosphorescent photosensitizer with hydrotalcites through firstly regulating layer microenvironment by coordination.

Author contributions

The manuscript was written through contributions of all the authors. All authors have given approval to the final version of the manuscript.

Conflicts of interest

The authors declare no competing financial interest.

Acknowledgements

We acknowledge grants from the National Natural Science Foundation of China (no. 52062025) and Gansu Key Research and Development Program Industrial project (22YF7GA137) and (23YFGA0041).

Notes and references

1 G. F. Li, D. X. Zhu, X. L. Wang, Z. M. Su and M. R. Bryce, Dinuclear metal complexes: multifunctional properties and applications, *Chem. Soc. Rev.*, 2020, **49**, 765–838.
2 S. Glass, M. Kühnert, N. Lippmann, J. Zimmer, R. Werdehausen, B. Abel, V. Eulenburg and A. Schulze, Photosensitizer-loaded hydrogels for photodynamic inactivation of multirestistant bacteria in wounds, *RSC Adv.*, 2021, **11**, 7600–7609.
3 K. Y. Zhang, Q. Yu, H. Wei, S. Liu, Q. Zhao and W. Huang, Long-lived emissive probes for time-resolved photoluminescence bioimaging and biosensing, *Chem. Rev.*, 2018, **118**, 177–1839.
4 I. Bhattacharjee and S. Hirata, Highly efficient persistent room-temperature phosphorescence from heavy atom-free molecules triggered by hidden long phosphorescent antenna, *Adv. Mater.*, 2020, **32**, 2001348–2001356.
5 W. P. Lustig, S. Mukherjee, N. D. Rudd, A. V. Desai, J. Li and S. K. Ghosh, Metal-organic frameworks: functional luminescent and photonic materials for sensing applications, *Chem. Soc. Rev.*, 2017, **46**, 3242–3285.
6 J. Li, X. X. Wang, G. X. Zhao, C. L. Chen, Z. F. Chai, A. Alsaedi, T. Hayat and X. K. Wan, Metal-organic framework-based materials: superior adsorbents for the capture of toxic and radioactive metal ions, *Chem. Soc. Rev.*, 2018, **47**, 2322–2356.
7 Y. X. Bian, X. J. Cai, Z. H. Lv, Y. M. Xu, H. Wang, C. L. Tan, R. Z. Liang and X. S. Weng, Layered double hydroxides: a Novel promising 2D nanomaterial for bone diseases treatment, *Adv. Sci.*, 2023, 2301806–2301835.
8 R. Gao, X. Mei, D. P. Yan, R. Z. Liang and M. Wei, Nano-photosensitizer based on layered double hydroxide and isophthalic acid for singlet oxygenation and photodynamic therapy, *Nat. Commun.*, 2019, **10**, 4247–4256.
9 L. Lv, Z. X. Yang, K. Chen, C. D. Wang and Y. J. Xiong, 2D Layered double hydroxides for oxygen evolution reaction: from fundamental design to application, *Adv. Energy Mater.*, 2019, **9**, 1803358.
10 R. Gao and D. P. Yan, Layered host–guest long-afterglow ultrathin nanosheets: high-efficiency phosphorescence energy transfer at 2D confined interface, *Chem. Sci.*, 2017, **8**, 590–599.
11 F. Gándara, J. Perles, N. Snejko, M. Iglesias, B. Gómez-Lor, E. Gutiérrez-Puebla and M. A. Monge, Layered rare-earth hydroxides: a class of pillared crystalline compounds for intercalation chemistry, *Angew. Chem., Int. Ed.*, 2006, **45**, 7998–8001.
12 F. X. Geng, Y. Matsushita, R. Z. Ma, H. Xin, M. Tanaka, F. Izumi, N. Iyi and T. Sasaki, General synthesis and structural evolution of a layered family of

$Ln_8(OH)_{20}Cl_4 \cdot nH2O$ (Ln = Nd, Sm, Eu, Gd, Tb, Dy, Ho, Er, Tm, and Y), *J. Am. Chem. Soc.*, 2008, **130**, 16344–16350.

13 L. L. Liu, W. S. Liu and Y. Tang, Research progress on the hybrid luminescent materials based on layered rare-earth hydroxides, *Sci. Sin.: Chim.*, 2015, **45**, 251–261.

14 L. L. Liu, M. H. Yu, J. Zhang, B. K. Wang, W. S. Liu and Y. Tang, Facile fabrication of color-tunable and white light emitting nano-composite films based on layered rare-earth hydroxides, *J. Mater. Chem. C*, 2015, **3**, 2326–2333.

15 T. T. Shen, Y. Zhang, W. S. Liu and Y. Tang, Novel multi-color photoluminescence emission phosphors developed by layered gadolinium hydroxide *via in situ* intercalation with positively charged rare-earth complexes, *J. Mater. Chem. C*, 2015, **3**, 1807–1816.

16 B. Y. Shao, X. B. Zhang, S. Sang, A. P. Guo, F. M. Cui and X. J. Yang, A novel layered rare-earth hydroxides/polyvinyl alcohol hydrogel with multicolor photoluminescence behavior, *Eur. Polym. J.*, 2021, **147**, 110324–110329.

17 D. K. Aleshin, M. A. Mashkovtsev, Y. A. Kuznetsova, V. N. Rychkov, A. F. Zatsepin and E. V. Gordeev, Fabrication of $(Y_{0.95}Eu_{0.05})_2O_3$ phosphors with enhanced properties by co-precipitation of layered rare-earth hydroxide, *J. Alloys Compd.*, 2019, **805**, 258–266.

18 J. Y. Li, J. H. Duan, Z. H. He, Y. J. Liao, X. H. Liu, P. F. Rong, G. Chen, H. Wan, Y. M. Huang and R. Z. Ma, Facile synthesis of organic–inorganic hybrid layered rare-earth hydroxide nanocone for multifunctional drug delivery system with fluorescence probe and simultaneous magnetic resonance imaging, *Adv. Opt. Mater.*, 2023, **11**, 2203146.

19 S. M. Borisov, R. Fischer, R. Saf and I. Klimant, Exceptional oxygen sensing properties of new blue light-excitable highly luminescent europium(III) and gadolinium(III) complexes, *Adv. Funct. Mater.*, 2014, **24**, 6548–6560.

20 Y. Y. Li, B. Yan and X. F. Qiao, Epoxidation of styrene catalyzed by mesoporous propylthiol group-functionalized silica supported manganese(III) salen complexes with different pore morphologie, *Microporous Mesoporous Mater.*, 2013, **169**, 60–66.

21 X. D. Zhao, J. P. Cao, J. Zhao, G. H. Hu and Z. M. Dang, A hybrid Mg–Al layered double hydroxide/graphene nanostructure obtained *via* hydrothermal synthesis, Chem, *Phys. Lett.*, 2014, **605–606**, 77–80.

22 L. J. McIntyre, L. K. Jackson and A. M. Fogg, $Ln_2(OH)_5NO_3 \cdot xH_2O$ (Ln = Y, Gd–Lu): a novel family of anion exchange intercalation hosts, *Chem. Mater.*, 2008, **20**, 335–340.

23 Y. H. Sun, N. K. Chu, Q. Y. Gu, G. H. Pan, G. B. Sun, S. L. Ma and X. J. Yang, Hybrid of europium-doped layered yttrium hydroxide and organic sensitizer – effect of solvent on structure and luminescence behavior, *Eur. J. Inorg. Chem.*, 2013, 32–38.

24 Q. Zhu, J. G. Li, C. Zhi, X. Li, X. Sun, Y. Sakka, D. Golberg and Y. Banbo, Layered rare-earth hydroxides (LRHs) of $(Y_{1-x}Eu_x)_2(OH)_5NO_3 \cdot nH_2O$ (x = 0-1): structural variations by Eu^{3+} doping, phase conversion to oxides, and the correlation of photoluminescence behaviors, *Chem. Mater.*, 2010, **22**, 4204–4213.

25 H. Q. Ma, Y. W. Xu, Q. G. Meng, L. L. Zhang, R. M. Wang and D. F. Sun, Synthesis, structure, and luminescent properties of three coordination compounds based on *in situ* generated tetrazolate and carboxylate ligands, *Z. Anorg. Allg. Chem.*, 2014, **640**, 1408–1412.

26 J. Yao, Q. Zhu and J. G. Li, Garnet transparent ceramic film of $Y_3Al_5O_{12}$:Eu^{3+} fabricated through an interface reaction of layered rare-earth hydroxide nanosheets on amorphous alumina, *Appl. Surf. Sci.*, 2022, **579**, 152226–152234.

27 M. Fernandes, Z. Bermudez, V. S. Ferreira, R. A. Carlos, L. D. Charas, A. Morgado, J. Silva and M. M. Smith, Highly photostable luminescent poly (epsilon caprolactone) siloxane biohybrids doped with europium complexes, *Chem. Mater.*, 2007, **19**, 3892–3901.

28 Z. L. Zhao, J. X. Ru, P. P. Zhou, Y. S. Wang, C. F. Shan, X. X. Yang, J. Cao, W. S. Liu, H. C. Guo and Y. Tang, A smart nanoprobe based on a gadolinium complex encapsulated by ZIF-8 with enhanced room temperature phosphorescence for synchronous oxygen sensing and photodynamic therapy, *Dalton Trans.*, 2019, **48**, 16952–16960.

29 W. Lv, Z. Zhang, K. Y. Zhang, H. Yang, S. Liu, A. Xu, S. Guo, Q. Zhao and W. Huang, A mitochondria-targeted photosensitizer showing improved photodynamic therapy effects under hypoxia, *Angew. Chem., Int. Ed.*, 2016, **55**, 9947–9951.

30 B. X. Sun, C. Wei, H. B. Wei, Z. L. Cai, H. Y. Liu, Z. Y. Zang, W. C. Yan, Z. W. Liu, Z. Q. Bian and C. H. Huang, Highly efficient room-temperature phosphorescence achieved by gadolinium complexes, *Dalton Trans.*, 2019, **48**, 14958–14961.